13 Computer Assisted Physics

P. F. Meier, R. M. Dünki, R. M. Füchslin, P. Hüsser, R. Luchsinger, H. R. Moser, S. Schafroth, J. M. Singer, E. Stoll

Introduction

The Computer Assisted Physics group has continued its research activities in computational physics. Selected examples of progress are presented in the following subsections. They comprise

(1) Quantum Monte Carlo simulations of the temperature dependence of the Knight shifts in high–temperature superconducting materials

(2) calculations of the electronic structure of the P–H complex in Si and the corresponding hydrogen vibrational modes

(3) a molecular dynamics study of the doping of high T_c superconductors with oxygen, a joint project with the MultiMediaLab (Institut für Informatik)

(4) a simulation of polymerisation which was started in collaboration with the Institute for Physical Chemistry

(5) an analysis of electroencephalograms in epilepsy by means of nonlinear dynamics, a study in collaboration with the Department of Neurology of the University Hospital.

13.1 Hubbard model predictions for the Knight shift in cuprates

NMR measurements of the Knight shifts K_s and the nuclear magnetic spin relaxation rates provide substantial information on the spin dynamics in the cuprate high-T_c superconductors. A comprehensive description of the different behaviors found in underdoped and overdoped compounds is considered as a stringent accessory to any theoretical understanding of these materials.

With the change of one control parameter, the charge carrier (hole) doping, these materials can be changed from insulating to metallic and superconducting to normal metallic. One of the key features of the underdoped regime is the opening of a gap in the spin and charge excitations at a temperature T^* well above T_c [1, 2, 3].

We performed Quantum Monte Carlo (QMC) simulations supplemented by Hartree-Fock (HF) calculations to investigate the static spin susceptibility in a two–dimensional tight-binding Hubbard model with attractive pairing interaction. Because of the simplicity (there are just two simple control parameters, doping and coupling strength) this model allows an easy investigation of several aspects of superconductivity. We use it to gain better understanding of the dependence of certain experimentally accessible quantities on the pairing mechanism.

The attractive Hubbard model is one of the simplest models for strongly correlated electron systems undergoing (i) a normal state to superconductor phase transition along the temperature axis for finite electron density ρ and coupling strength

U and (ii) for $T = 0$ an insulator to superconductor to normal metal transition along the $1/U$ control parameter. Our intention is to use the QMC method for an exact treatment, in particular in the region around the phase transition, where mean-field approaches fail, and to supplement the simulation results by an approximate treatment where it is suitable. This allows us to describe cuprate superconductors not only in the over- and optimally doped regime (in phase transition terminology: the regime closer to the normal metal), but access also many interesting properties observed in underdoped materials (which are in the regime closer to the superconductor-insulator transition). The QMC treatment with onsite coupling produces an s-wave superconducting state only, whereas within the HF treatment an extension to a momentum dependent interaction and gap is easily possible. Both techniques provide the static magnetic susceptibility; we calculated the ratio $K_s(T)/K_s(T_c) = \chi_s(0,0,T)/\chi_s(0,0,T_c)$.

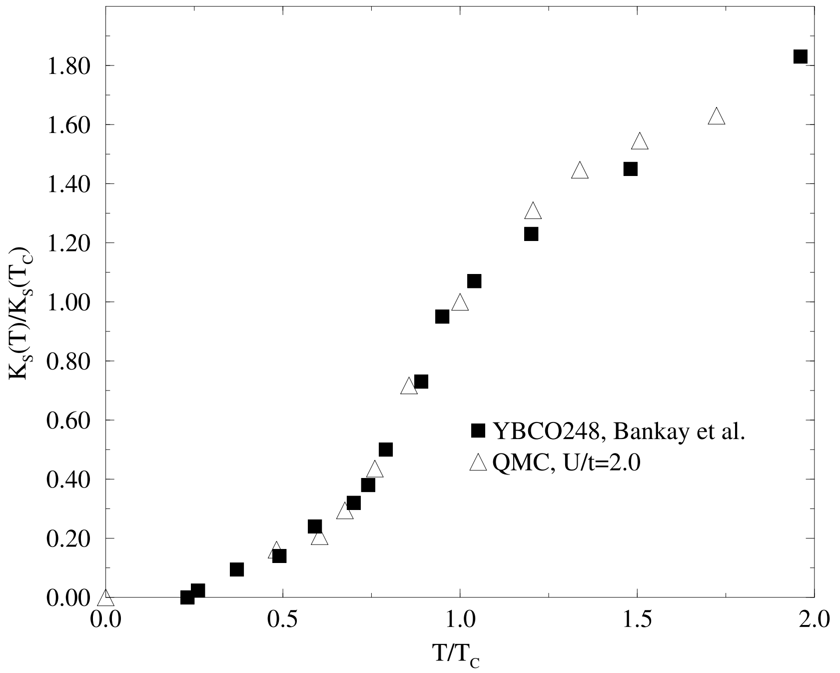

Figure 13.1: Knight shift $K_s(T)/K_s(T_c)$ vs. normalized temperature T/T_c, $YBa_2Cu_4O_8$ (underdoped) from Bankay et al. [2] and QMC-data, attractive Hubbard model, $U/t = 2.0$.

In 13.1 we present data from our model calculations and compare them to measurements in the underdoped stoichiometric material $YBa_2Cu_4O_8$ from Bankay et al. [2]. We are able to reproduce the experimental data by QMC results, with the coupling strength as the only fitting parameter. In contrast, a mean-field approach is not able to reproduce the behavior at T_c and in the normal state correctly. Especially the normal state decrease above T_c in case of the underdoped materials, usually referred to as a 'spin-gap', is reproduced. Nevertheless, below T_c there are certain deviations, since the QMC data are based on an onsite pairing interaction and thus s-wave superconductivity. The extended HF formalism, however, with an appropriate interaction to produce d-wave pairing is able to correctly reproduce the superconducting state.

13.2 Fermi Resonance of Hydrogen in Phosphorus doped Silicon

The passivation of defects and impurities in semiconductors by hydrogen has been investigated intensely in recent years. Studies of the hydrogen vibrations of the defect complexes, coupled with theoretical calculations, have been responsible for much of the rapid progress in this field. The determination of the structure of donor-H complexes in Si has provided an example of the power of this approach. The hydrogen vibrational spectra of donor-H complexes in Si consists of three bands observed near 810, 1560, and 1660 cm^{-1}. The two former bands were assigned to the H-wagging and stretching mode, respectively, while the assignment of the 1660 cm^{-1} band has been controversial. In a recent paper [4] it was argued, based on experimental results, that if the second harmonic of the wagging mode and the H-stretching fundamental mode were weakly coupled by anharmonic interactions, the origin of the 1560 and the 1660 cm^{-1} band can be explained by a Fermi resonance between the second harmonic of the wagging mode and the fundamental stretching mode. Based on this model, the assignment of all the observed hydrogen vibrational bands was possible for the first time.

While in previous theoretical studies [5] possible couplings between wagging and stretching mode were neglected, we have in a recent work for the first time investigated these coupling effects. To this end, a P-H complex in Si was studied. In a first step the equilibrium geometry was calculated with cluster methods. The energy surface in the vicinity of H was then determined. By assuming rotational symmetry around the longitudinal (stretching) axis, the numerical costs could be heavily reduced. We showed that the energy surface can be extremely good approximated by a simple analytical form based on a Morse potential in the longitudinal direction and a harmonic potential in the transverse (wagging) direction. Without coupling the Schrödinger equations for the H-impurity were solved analytically. The coupling terms of the potential were then treated by perturbation theory.

Without coupling effects we obtained bands at 1631 and 1686 cm^{-1}. Inclusion of the coupling terms leads to frequencies of 1546 and 1678 cm^{-1} (i.e. very close to the experimental results) and a strong mixing between the wagging and the stretching mode was found as it is typical for a Fermi resonance (see 13.2). Thus the proposed explanation of the vibrational spectra of donor-H complexes in Si is fully confirmed by our theoretical investigations.

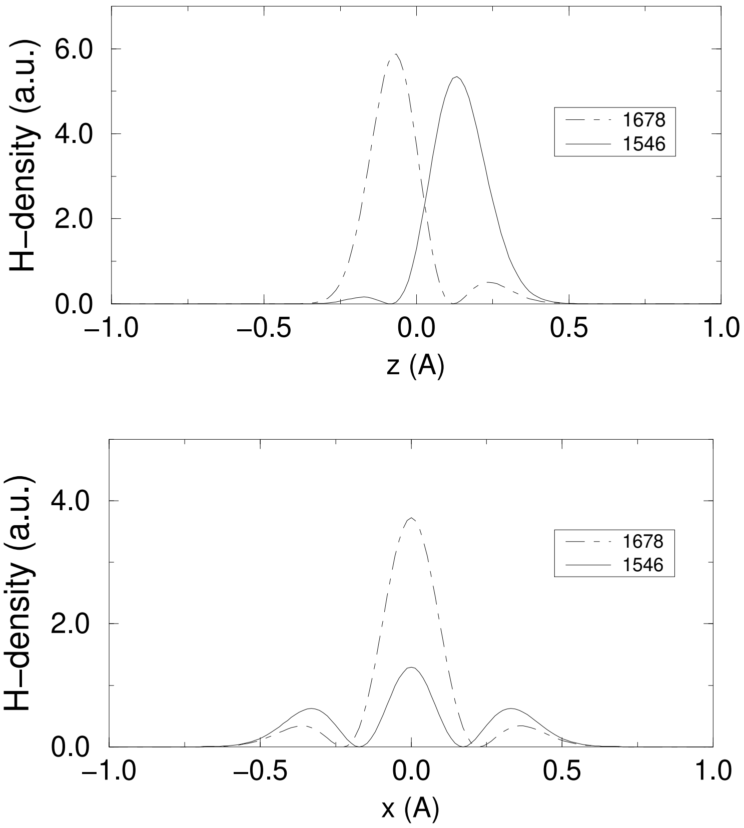

Figure 13.2: Square of the hydrogen wave–function of the 1546 and 1678 cm^{-1} bands calculated by perturbation theory. The projection onto the longitudinal (transverse) direction is shown in the upper (lower) figure. Distances are given in Å.

13.3 Doping high T_c superconductors with oxygen and metallic atoms: a molecular dynamics study

The magnetic and superconducting properties of high-T_c superconductors depend very heavily on the oxygen content of these compounds. This content can be controlled by the pressure of the ambient oxygen atmosphere depending on the temperature of synthesis and sample annealing.

To simulate this experimental behavior by the Interactive Molecular Dynamics System (IMDS) package [6], an array of YBCO unit-cells is investigated based on a simplified net interaction with repulsive and attractive forces of the type $V(d_{ij}) = 4\,[\,|\epsilon\,|\,(\sigma/d_{ij})^{12} - \epsilon\,(\sigma/d_{ij})^6]$, where σ and ϵ are tunable parameters and d_{ij} denotes the interatomic distance between the atoms i and j. A proper choice of these parameters allows the identification and reproduction of known stable YBCO-structures.

Based on this work, we are able to study the influence of new metal and oxygen dopant atoms and defects. By adding or removing particles on different sites of the sample using a recently implemented new picking mechanism, the variation of the ground state energy is calculated. Equilibrium of these new materials is reached by minimizing the kinetic energy of these samples with a simulated annealing algorithm [6]. The cooling speed of the annealing procedure is also determined interactively and the behavior of the system is controlled visually.

13.4 "Living" radical polymerization

Since the first report of "living" high polymers with low polydispersity and controllable molecular weight produced by thermal radical initiation, the field of "living" radical polymerization has been advanced tremendously both in science and industry. In contrast to conventional radical polymerization, one of the possible radical radical reaction is suppressed. Consider an initiator S = x—y which decays into x· and y· due to thermal or photochemical activations. These free radicals react very fast and form species x—x, y—y and x—y = S. Since the decay of S is very slow compared to the recombination, most of the free radicals disappear before a monomere addition can take place. If the formation of y—y is suppressed, the y· radicals stay alive. A salient feature of this living radical polymerization is the growth of chains with sharply peaked molecular weight distributions.

The kinetics of the system can be modeled by a set of ordinary first order differential equations. This allows to conveniently explore various combinations of reaction rates. We started a collaboration with the physical chemistry institute to support their experiments and their analysis [7] of the self–regulation of the reaction system with large–scale numerical simulations.

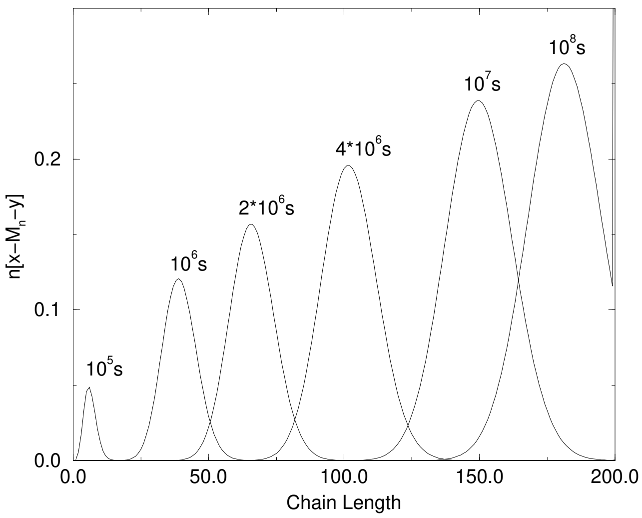

Figure 13.3: Time evolution of the molecular weight distribution of the species x–M_n–y prepared using living radical polymerization.

A typical evolution of the molecular weight distribution is shown in Fig. 13.3. The mean value of the distribution is moving towards longer chains as time proceeds. Also the width is quite small, corresponding to a polydispersity around one whereas conventional radical polymerization amounts in polydispersities around four. As can be seen from the figure the time scale is still well beyond the limits for industrial application. Optimization of the system parameters is subject for further investigations. Despite these difficulties living radical polymerization is a key tool for the development of novel polymer materials with improved physical and chemical properties.

13.5 Electroencephalograms in epilepsy: Analysis and seizure prediction by means of nonlinear dynamics

Epileptic seizures represent a quite frequently occurring malfunction of the central nervous system. Therefore the search for precursors of a seizure is of utmost clinical relevance and even may guide us to a deeper understanding of the seizure generating mechanisms. On this score we extracted Lyapunov exponents and related quantities from intracranial electroencephalograms (EEGs), an approach that proved useful and predicative in the studies we performed up to now.

The project is necessarily an interdisciplinary one that essentially splits into (A) diagnostic research as well as data acquisition, and (B) time series analysis and interpretation of the characteristic quantities that have been extracted from the raw data. Therefore we initiated a close collaboration between the University Hospital Zurich, Department of Neurology, and our Physics Institute.

Since most of the techniques developed within the field of nonlinear dynamics suffer from a high (and generally unknown) noise–level inherent in empirical time series, the use of high quality input data is a major issue. In particular, this applies to physiological data that frequently even appear to be non–stationary. However, the intracranial EEGs (invasive and semi–invasive methods) recorded in the group around Prof. H.G. Wieser at the University Hospital provide a standard that is clearly beyond the usual monitoring of EEGs directly from the surface of the skin. We then of course selected and adapted our numerical methods according to this opportunity.

The problem of seizure prediction has been tackled for many years, particularly by looking for so called preictal (i.e., before the onset of seizure) changes in an EEG. One of the approaches reveals some indication that the correlation dimension (D_2) slightly decreases already significantly prior to a seizure onset, see, e.g., [8]. However, we found that much more sensitive indicators for preictal changes can be selected, namely both Lyapunov spectra (i.e., the density of Lyapunov exponents), and spectra of local expansion exponents [9].

In Fig. 13.4 we would like to present an example. Intracranial EEGs with 9 bipo-

Figure 13.4: Four spectra of local expansion exponents originating from different time windows of an intracranial EEG (9 suitably filtered bipolar signals, primary epileptogenic area). Dashed: ca. 28 min before onset of seizure; dotted: ca. 14 min before onset of seizure; dash-dotted: the interval 95 − 5 sec before onset of seizure; full: within the ictal phase. We have chosen to use those local exponents that in a time average lead to the largest Lyapunov exponent. (right): As left hand side, but the data originate from the non–primary epileptogenic area. Compared to the left hand side, the full curve (ictal phase) has been omitted because of a strong non–stationarity of the corresponding signal.

lar channels have been analyzed in the following manner. During a time window of 90 seconds, corresponding to 90 x 200 = 18000 data points the signals were assumed to be stationary. (This was confirmed by visual inspection and by separately analyzing the first and second half of the time series.) The left hand part of Fig. 13.4 presents four spectra of local expansion exponents, all the 9 signals from the "primary epileptogenic area" being analyzed simultaneously (no delay embedding). Two curves represent the situation some 28 and 14 minutes before the beginning of the seizure, respectively. One spectrum characterizes the interval up to some 5 seconds before the onset of the seizure while the fourth one has been recorded during the ictal phase. Expectedly, the first two spectra show an overall agreement. The third one, originating from a visually very similar time series, exhibits a dramatic change in its spectral shape. Finally, the fourth one that stems from the ictal phase reverses the change and again differs from all the other ones. However, it has been known for a long time that a seizure is attended with a clearly visible alteration of the EEG (namely a strong increase of regularity and decrease of D_2), and so the change in the corresponding spectrum does not astonish.

Fig. 13.4 (right hand part) represents the same situation for the non–focal side. This time the ictal spectrum is missing since the corresponding signal is strongly non–stationary. Again we note a preictal change that, expectedly, is less pronounced compared to the primary epileptogenic area. Additionally, the Lyapunov spectra confirm the above observations, partly because the Lyapunov exponents of course are closely related to the spectra of local expansion exponents.

At the present stage we think that our spectral methods exhibit quite a strong forecasting power that may well prove superior to previous approaches. In particular, the degree of irregularity and of dissipation becomes quantitatively known. This then allows us to tackle an old and challenging problem within the field of nonlinear dynamics, namely the quantitative distinction and characterization of high–dimensional "real life" signals. This is of particular interest in cases like the preictal signals described above, where a visual inspection and comparison cannot reveal the relevant properties.

References

[1] J. M. Singer et al., Phys. Rev. B **54**, 1286 (1996).

[2] M. Bankay et al., Phys. Rev. B **50**, 6416 (1996).

[3] T. Schneider et al., submitted to Europhys. Lett. 1997; J. M. Singer et al., unpublished 1997; J. M. Singer et al., Physica B (1997).

[4] J.-F. Zheng and M. Stavola, Phys. Rev. Lett. **76**, 1154 (1996).

[5] Yu Zhou, R. Luchsinger and P.F. Meier, Phys. Rev. B **51**, 4166 (1995)

[6] C. Stern, P. Stucki, and E. Stoll, Proc. Information Conf. Module 3 Mass. parall. syst., eds. K. Bauknecht and J.M. Grossenbacher, (Swiss Nat. Sci. Fond., Bern, 1994), pg. 29.

[7] H. Fischer, J. Am. Chem. Soc. **108**, 6446 (1988).

[8] C.E. Elger and K. Lehnertz, *Epileptic seizures and syndroms*, ed. P. Wolf (John Libbey and Company Ltd, London, 1994) p. 541.

[9] H.R. Moser, P.F. Meier, and F. Waldner, Phys. Rev. B **47**, 217 (1993).